ISSN 1063-7745, Crystallography Reports, 2022, Vol. 67, No. 7, pp. 1068–1074. © Pleiades Publishing, Inc., 2022.

DIFFRACTION AND SCATTERING OF IONIZING RADIATIONS

On the Theory of X-ray Diffraction Interferometry in Single Crystals. Peculiarities of Effect and Possibilities of Application

V. G. Kohn[a] and I. A. Smirnova[b,*]

[a] *National Research Centre "Kurchatov Institute," Moscow, 123182 Russia*

[b] *Institute of Solid State Physics, Russian Academy of Sciences, Chernogolovka, Moscow oblast, 142432 Russia*

**e-mail: irina@issp.ac.ru*

Received June 2, 2022; revised June 2, 2022; accepted June 8, 2022

Abstract—A new version of X-ray diffraction interferometer in a single crystal is studied theoretically. This device is similar to the Young interferometer with two slits, but, instead of slits, it is proposed to use a bilens interferometer based on compound refractive lenses, which have already been created and are used in practice. The crystal makes it possible to reduce radically the interferometer sizes and provides additional possibilities for increasing the measurement accuracy. The features and structure of interference fringes, as well as the possibilities of practical use of the new-type interferometer are analyzed. Numerical calculations were performed using a universal computer program, which is being developed to solve a wide range of problems in X-ray optics.

DOI: 10.1134/S1063774522070446

INTRODUCTION

Visible-light interferometers belong to the most accurate instruments for measuring physical constants. In particular, the Michelson interferometer was used to prove the theory of relativity and constancy of speed of light at any speed of the source. Many different types of interferometers are used in science and technology; however, the most popular is the simplest one, specifically, the double-slit interferometer, known as the Young interferometer [1]. If a plane monochromatic wave with a wavelength λ is incident on a slit with a width d, the radiation transmitted through the slit acquires angular divergence with a width $\alpha = \lambda/d$. This effect is known as diffraction.

Under conditions of double-slit diffraction, the beams from the slits begin to intersect at a distance $z_0 = x_0/\alpha$ along the optical axis, where x_0 is the distance between the slits in the transverse direction. The phase relations in different beams are matched for coherent radiation. Therefore, addition of the fields from two slits leads to the occurrence of interference fringes with a period $p = \lambda z_1/x_0$, where $z_1 > z_0$ is the distance from the slits to the detector.

The development of interferometry in X-ray optics was held back for a long time by the absence of coherent sources (more exactly, by their fairly small coherence length and insufficiently high brightness). The situation changed in the middle of the 1990s due to the development of third-generation synchrotron radiation (SR) sources; the first of them was the facility in Grenoble (France). These sources have a sufficient brightness and high coherence. To date, many studies devoted to different versions of X-ray interferometry have been published. The most interesting interferometers based on planar compound refractive lenses (CRLs) for SR sources and X-ray free-electron lasers were described in [2–7]. The term "CRL" was introduced in the pioneer work [8].

The specificity of X rays is that they make it possible to develop radically new interferometry based on the X-ray diffraction from the lattice in single crystals [9]. In the case of a double-slit interferometer, the beams must have sufficiently high angular divergence and intersect at a distance as small as possible. Without crystals, this is difficult to implement for hard X-rays because of their very small wavelength λ.

The situation can be improved using two-wave Laue diffraction from a single-crystal lattice. In this case a narrow beam exposes the so-called Borrmann fan with a vertex angle $2\theta_B$, where θ_B is the Bragg angle, which may take any value from 0° to 90°. This fact was experimentally revealed for the first time in [10] and explained theoretically in [11, 12]. The beams from two slits may interfere in a crystal less than 1 mm thick, forming periodic fringes with high and low intensity.

X-ray diffraction interferometry (XDI) in a single crystal was described theoretically for the first time in [13] for the double-slit scheme (analogue of the Young interferometer); the following analytical formula was derived for the interference-fringe period:

$$p = 2\Lambda t \tan^2(\theta_B)/x_0, \quad (1)$$

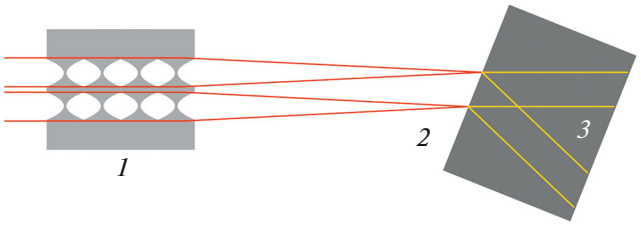

Fig. 1. The main part of the possible schematic of the experiment: (*1*) bilens interferometer based on planar CRLs, (*2*) single crystal, and (*3*) beam overlap region.

where x_0 is the distance between the slits, $\Lambda = \lambda\cos(\theta_B)/|\chi_h|$ is the extinction length, t is the crystal thickness, and χ_h is the diffraction parameter. The parameters p and x_0 are measured in the direction parallel to the crystal surface.

This statement of the experiment deserves attention; nevertheless, it has a number of drawbacks. The main is that only a very small fraction of incident beam intensity is used in any double-slit experiment, and the luminosity is low for this reason. Another type of interferometer was proposed in [14], in which spatial beam separation occurs in the air gap between two crystal blocks. The point is that the diffraction from a single crystal lattice forms at once two beams (direct and reflected).

In addition, there is a diffraction focusing effect, which was first predicted theoretically in [15, 16] and then revealed experimentally in [17–19]. This effect was investigated later [20, 21] for the case of diffraction from two successive crystals separated by a large distance. When using the diffraction focusing effect, an analogue of the Young interferometer is implemented in the second block after spatial separation of the beams focused in the first block.

It was noted in [14] that an interference pattern is obtained even without beam focusing. It is fairly simple to separate beams in space using an air gap between two blocks. It is of interest that an experiment of this type was already performed more than 50 years ago [22], and interference fringes were observed. However, this method was not developed at that time.

In this paper we discuss another way to improve the model of double-slit interferometer proposed in [13]. The idea is to align a two-lens interferometer based on planar CRLs with diffraction in a crystal. A two-lens interferometer can form an interference pattern in space without a crystal, as was clearly demonstrated in [2, 3, 7]. However, the pattern is observed at a rather large distance from the interferometer. This distance can be reduced to zero using a crystal. In addition, this approach allows one to study the parameters of the crystal itself.

In this work we analyze also the possibility of measuring accurately the refractive indices of different materials using the new-type interferometer, based on the shift of interference fringes, as well as the new type of imaging microscopic objects and gas capsules in crystals.

SCHEMATIC OF THE EXPERIMENT AND METHOD OF NUMERICAL CALCULATION

Figure 1 shows the main part of the experimental scheme that can be implemented on SR beamlines. It is assumed that the radiation from a source passes through a monochromator (omitted in Fig. 1), which selects the necessary wavelength, and then is focused by a bilens interferometer (*1*) at two points on the crystal surface. The crystal (*2*) is oriented so that its reflecting planes make a Bragg angle θ_B with the principal beam direction, an a triangular region with an angle $2\theta_B$ is exposed in the crystal. In the symmetric case (considered here) these planes are oriented perpendicular to the input crystal surface.

When a crystal is illuminated with a CRL-based interferometer, the regions of illumination from different foci overlap at some distance from the surface, and a region is formed in which both beams interfere (*3*). It is reasonable to place a detector (is not shown) as close as possible to the output crystal surface. This must be done to reduce the influence of the SR spectral width after the monochromator. The point is that the Bragg angle changes with a change in wavelength, which leads to the undesirable effect of shifting the entire pattern in the perpendicular direction when the distance between the crystal and detector is fairly large.

The experiment was simulated using the universal computer program XRWP1 [23], developed to study theoretically various experimental schemes on SR sources. The methods for simulating different schemes of phase contrast and SR beam focusing using the refraction effect [24] and diffraction in single crystals have been developed most thoroughly.

The program implies that a narrow SR beam passes along an almost straight-line path from a source (having small transverse sizes) to a coordinate detector, measuring the intensity distribution in the transverse plane. The Z axis of the Cartesian coordinate system coincides with the beam propagation direction. The two-wave diffraction in crystal and planar CRLs change the intensity distribution in the XZ plane, whereas no changes occur along the Y axis. For this reason we will consider only the dependence on the coordinate x along the X axis.

If the CRL focal length exceeds several times the CRL length or is even larger, one can apply with reasonable accuracy the approximation of phase contrast theory, where one CRL is described by the transmission function $T(x)$:

$$T(x) = \exp(-iK[\delta - i\beta]t(x)),$$
$$t(x) = N(t_0 + x^2/R). \quad (2)$$

Here, $K = 2\pi/\lambda$ is the wave number; $\delta - i\beta = 1 - n$, where $n = \chi_0/2$ is the complex refractive index, taking into account also the absorption of the beam propagating through the crystal; $t(x)$ is the thickness of the CRL material for the ray with a coordinate x; R is the curvature radius of the parabolic surface of one CRL element; t_0 is the thickness of the thin layer of material between the two surfaces; and N is the number of biconcave CRL elements.

Equation (1) is applicable for the region satisfying the condition $|x| < x_a$, where x_a is half of the CRL aperture. Another equation is valid in the region $|x| > x_a$: $T(x) = T(x_a)$ (if the incident beam is wide). The CRLs are often accompanied by a slit which opens only the apertures. Then $T(x) = 0$ for the regions closed by the slit.

Let us denote the wave function (WF) of the radiation incident on the interferometer as $E_0^{(0)}(x)$. This may be the transverse part of a spherical wave from a point source or a more complex function, taking into account the change in the WF after its transmission through the objects installed on the path from the source to the CRL. The equation for the WF directly after the bilens CRL-based interferometer has a relatively simple form:

$$E_0^{(1)}(x) = [T(x - x_s/2) + T(x + x_s/2)]E_0^{(0)}(x), \quad (3)$$

where x_s is the distance between the CRL centers in the interferometer.

The change in the WF during propagation of radiation in empty space along the Z axis is described based on the Huygens–Fresnel principle and reduced to calculation of the convolution of the WF with the Fresnel propagator. All convolutions in the program are calculated by the Fourier transform method. The convolution of two functions in real space is known to be equivalent to their product in reciprocal space. The Fourier transforms of the functions will be denoted by the same letters, but the argument will be q.

Correspondingly, the WF at some distance z_1 from a CRL has the following Fourier transform:

$$E_0^{(2)}(q) = P(q, z_1)E_0^{(1)}(q). \quad (4)$$

The Fourier transform of the Fresnel propagator has the analytical form

$$P(q, z) = \exp(-i(\lambda z/4\pi)q^2). \quad (5)$$

It is also convenient to describe the diffraction of radiation from a single crystal lattice in reciprocal space, i.e., for plane waves. In this case, the WF of the incident radiation is transformed into a vector function consisting of two components: along with the incident wave there arises a reflected wave, whose direction differs by the angle $2\theta_B$ from the incident wave direction. In this study we analyze specifically the reflected wave, which arises for monochromatic radiation only when the crystal is correctly oriented.

At the crystal output this wave has the following Fourier transform:

$$E_1^{(3)}(q) = F(q)M_{10}(q, t_c)E_0^{(2)}(q). \quad (6)$$

Here, t_c is the crystal thickness, and the matrix element of transition from transmitted to reflected wave has the analytical form [14]

$$M_{10}(q, t_c) = (X_h/2g)[\exp(iA + iG) - \exp(iA - iG)], \quad (7)$$

where

$$A = (X_0 + \alpha_q)t_c/2\gamma_0, \quad g = (\alpha_q + X^2)^{1/2}, \quad (8)$$

$$G = gt_c/2\gamma_0, \quad X = (X_h X_{-h})^{1/2},$$
$$\alpha_q = (q - q_0)\sin(2\theta_B). \quad (9)$$

Here, $X_{0,h,-h} = K\chi_{0,h,-h}$, $\chi_{0,h,-h}$ are the diffraction parameters, i.e., the Fourier components of the crystal polarizability on the reciprocal lattice vectors $\mathbf{0}$, $\mathbf{h}$, $-\mathbf{h}$; $q_0 = K\theta_0$; θ_0 is the angular deviation of crystal from the Bragg angle; and $\gamma_0 = \cos\theta_B$.

The coordinates x and q in all equations are counted in the direction perpendicular to the SR beam direction. As was noted in [14], the function in reciprocal space must be additionally multiplied by the phase factor

$$F(q) = \exp(-iqt_c \sin\theta_B) \quad (10)$$

to make the Borrmann fan center coincide with the origin of coordinates.

The dependence $E_1^{(3)}(x)$ is obtained from $E_1^{(3)}(q)$ using the inverse Fourier transform. The direct and inverse Fourier transforms are calculated on point grids with a constant spacing. The number of grid points is $n = 2^k$, where k is an integer. The spacings in direct and reciprocal spaces (d_x and d_q, respectively) are related as follows: $d_x d_q = 2\pi/n$. This is necessary for using the fast Fourier transform method [25] in its optimal version, although sometimes the number of points may be rather large. In this study we consider the coordinate dependence of the reflected beam intensity at the crystal output, i.e., the function $I_1(x) = |E_1^{(3)}(x)|^2$. The number of points for the plot in a specified interval can easily be obtained by interpolation from the calculation array.

CALCULATION RESULTS AND DISCUSSION

Among the existing bilens interferometers for XDI, the most appropriate is the first one, which was presented in [2]. CRLs are made of silicon, with a length of one element of 102 μm, an aperture $A = 50$ μm, and a curvature radius $R = 6.25$ μm. The distance between the centers of two CRLs is $x_s = 60$ μm. Calculation

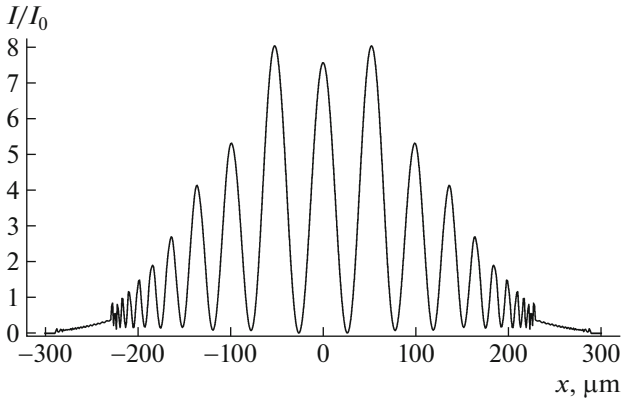

Fig. 2. Intensity distribution in the beam overlap region for a 0.8-mm-thick silicon crystal; reflection 220; photon energy 10 keV; and CRLs with an aperture of 50 μm, a curvature radius of 6.25 μm, and a distance between centers of 60 μm (see details in text).

was performed for a silicon single crystal, photon energy $E = 10$ keV, and reflection 220. In this case, $\theta_B = 18.8°$, and the CRL focal length is 6.33 cm. The diffraction parameters $\chi_{0,h,-h}$ were obtained using the on-line program reported in [26].

Figure 2 shows the intensity distribution in the reflected beam directly at the output of a crystal of thickness $t_c = 0.8$ mm. A point grid with $n = 2^{15} = 32768$ and $d_x = 0.02$ μm was used for calculation. The coordinate x is counted in the direction perpendicular to the beam direction. The distances in this direction are obtained from the distances along the crystal surface as a result of multiplying by the factor $\cos\theta_B$. Correspondingly, the Borrmann fan base is $2t_c\sin\theta_B = 517$ μm. The interference region size is 60 μm smaller.

The simplest interference fringes were obtained for relatively thick crystals, when the field with a large absorption coefficient has a very small amplitude. As a result, there remains only the field for which standing wave nodes are located between atoms and the absorption sharply decreases (the Borrmann effect [27]). In this case the maximum intensity for one narrow beam corresponds to the middle of the Borrmann fan base, and the intensity decreases during the motion to edges [14].

The maximum oscillation amplitude is obtained approximately at the center of the overlap region. The parameter I_0 in Fig. 2 is equal to 2×10^{-4} if the radiation intensity before CRL is assumed to be unity. The intensity loss is due to the interference of rays with a relatively large absorption coefficient in the crystal. An interesting feature of XDI is the variable oscillation period. Equation (1) for the oscillation period (see above) is valid for only the central part of the XDI region. In this case it has the form

$$p = 2\lambda t_c \cos\theta_B (\sin\theta_B)^2 \left(|\chi_h| x_s\right)^{-1}. \quad (11)$$

Substituting numerical values of all parameters, we obtain $p = 54.4$ μm, which is in good agreement with the calculation result (Fig. 2).

In Fig. 2 one can easily find both the total size of the interference region, equal to ~460 μm, and the total size of the illuminated region in the Borrmann fan, equal to ~580 μm. The intensity beyond the latter region is zero. One can also see that the central peak is lower than the neighboring ones. In the case of double-slit diffraction this does not hold true: the central peak is always higher. The reason for this anomaly is the same as for the interference in air [7]. The point is that the intensity of the beams decreases because of their large divergence at the focus: it becomes comparable with the intensity of the radiation passing through the bridge between the CRL aperture edges; the width of this bridge is 10 μm. This additional radiation distorts the central interference peaks, and they acquire a more complex shape.

Another feature of XDI is that one cannot obtain many interference bands by varying parameters. For example, the period decreases with an increase in the distance between sources (foci). However, the overlap region also decreases in this case (at reasonable crystal thicknesses). At the same time, the period decreases linearly with a decrease in wavelength λ. But the width of the illuminated region decreases in the same way in this case.

From the point of view of practical application of this interferometer, it is useful to have a sufficiently large period, which can be measured with high accuracy. The resolution of modern coordinate detectors may be better than 1 μm. If all other parameters are known independently, measurements of the period can be used to calculate directly the diffraction parameter for the crystal in use. This is possibly not so interesting because the crystal should have a perfect lattice, and such crystals (silicon, germanium) have been studied well.

A more interesting fact is that the interferometer makes it possible to measure the phase shift when a narrow beam passes through a layer of any material. An object can be installed before the crystal at one of the interferometer foci. Figure 3 shows the structure of interference fringes for the case where the phase in the left beam changed by $-\pi$. Specifically, in the calculation, an object in the form of a boron fiber with a round cross section and diameter of 13.78 μm was installed before the crystal. Since the fringes in the two-dimensional pattern are obtained in the form of vertical bands with a height equal to the CRL etch depth (70 μm for the interferometer under consideration), the object can be inserted at the middle of this height, and the fringe shift will clearly be seen in the pattern recorded by the detector.

It is of interest that, when the fringes undergo a shift, their number on the left and on the right remains the same, but the symmetry is violated. The left peak

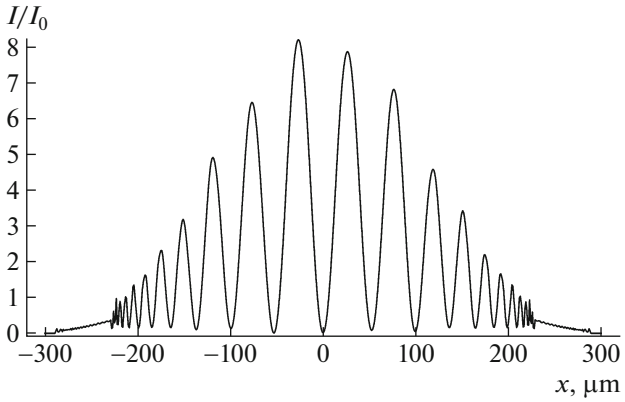

Fig. 3. Intensity distribution in the beam overlap region for the same parameters as in Fig. 2 at a phase shift of the radiation WF in the left focus by $-\pi$.

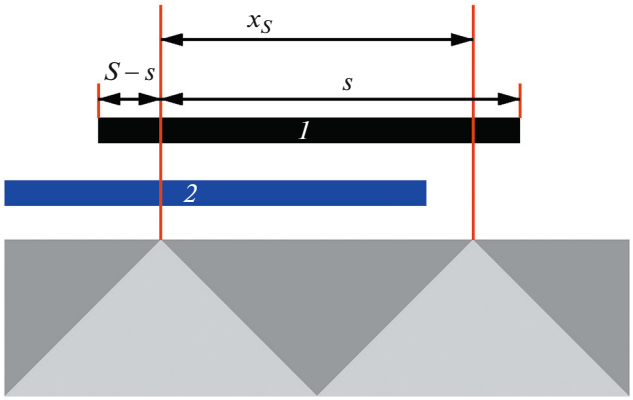

Fig. 4. Schematic showing coordinates when scanning object along the crystal surface. Illustration of the method for determining the dependence of object thickness during object scanning.

becomes higher than the right one. The reason in the same as in the case considered above, i.e., the presence of a bridge between the CRL aperture boundaries. Another specific feature of XDI is the fact that, when the phase shift in the left beam is negative, the peaks also shift to the left, whereas in air peaks shift to the right. The point is that the Fresnel propagator increases the phase with an increase in the beam path length, whereas the propagator crystal, vice versa, has the maximum phase at the center of the Borrmann fan, and the phase decreases when moving to its edges. For this reason, while the phase in the left beam decreases when the latter enters the crystal, the point at which this decrease is compensated is closer to the center of the left Borrmann fan. Accordingly, the central peak, corresponding to the equality of phases of the beams from two foci, shifts to the left, and its height increases.

The possibility of measuring the band shift with a change in the phase difference between the beams in the left and right interferometer arms gives rise to another version of the phase contrast method, in which the inverse problem is solved extremely easily. If the chemical composition of an object is known, the shift of the interference bands depends on only the difference in the object thicknesses at the points of object illumination by narrow beams before entering the interferometer crystal. Shifting the object in the direction perpendicular to the beam axis or simply along the crystal surface, one can record a coordinate dependence of the difference in thicknesses.

Let the origin of coordinates on the X axis correspond to the left beam, the object have a transverse size S, and the distance from its right edge to the left beam be s. The band shift to the left is proportional to the difference in the object thicknesses in the left and right beams: $\Delta = t_o(0) - t_o(x_s)$. When the object moves from left to right, the difference is zero if $s < 0$. In this case the object does not intersect the beams. In the range $0 < s < x_s$ the object intersects only the left beam, and the difference is $\Delta = t_o(0)$. In this case we obtain at once the object thickness at a distance $(S - s)$ from its left edge. Thus, this method makes it possible to determine the object thickness in the range from $(S - x_s)$ to S.

The situation is illustrated by Fig. 4. The above-described case refers to the object position denoted as *2*. In the range $x_s < s < S$ the object intersects both beams. This situation is denoted as *1*; it may occur only at $x_s < S$. In this case the object thickness at a distance $(S - s)$ from the left edge is calculated by subtracting Δ from the thickness at a distance $(S - s + x_s)$, which is known from previous measurements. Hence, the thickness in the range from 0 to $(S - x_s)$ can be determined. Thus, one can determine the thickness of an object on its entire transverse size. If $S < x_s$, it is sufficient to scan the object before the left beam. The obtained coordinate dependence of thickness can be used to determine the internal object structure using tomography [28] in the following way: to collect the coordinate dependences of thickness while rotating the object in the range from 0° to 180° with a small step.

This method is most preferred for studying micropores in crystals of silicon carbide (SiC) [29], sapphire (Al_2O_3), and some other compounds. The point is that pores are often very small, and magnification must be applied to determine their transverse sizes. In this technique the detector measures the longitudinal size, while the transverse size is measured by simple object displacement. Magnification for the longitudinal size can be implemented due to the larger fringe shift. In particular, the fringe shift with a change in the phase by π can be increased when passing to higher diffraction orders.

Figure 5 shows the calculation results for reflection 440, with the same values of other parameters. In this calculation the grid spacing is $d_x = 0.04$ μm. Curve *1*

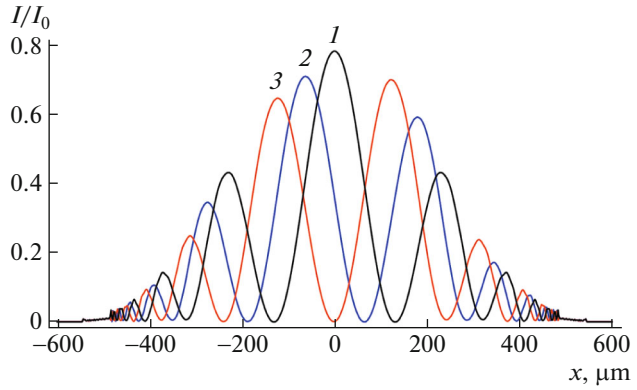

Fig. 5. Intensity distribution in the beam overlap region for the same parameters as in Fig. 2 but for reflection 440. The WF phase shift in the left focus is 0, $-\pi/2$, and $-\pi$ for curves *1*, *2*, and *3*, respectively.

corresponds to zero phase difference. In this case the Bragg angle is $\theta_B = 40.22°$, and the oscillation period is 275 μm, i.e., larger by a factor of 5 than for reflection 220 at the same crystal thickness. However, the intensity decreased by a factor of 10, because the I_0 value is the same as in Figs. 2 and 3. The curve is symmetric, and the number of interference fringes is fairly small.

Curve *2* corresponds to the WF phase shift by $-\pi/2$ in the left focus. Curve *3* corresponds to the shift by $-\pi$. It is of interest that the asymmetry of the second and third curves turned out to be opposite. The left peak is larger than the right one at small shifts, and vice versa at large shifts. The calculation results clearly show that, despite the very small number of interference fringes, measurement of their shifts makes it possible to determine with high accuracy the small phase shift formed by a microscopic object.

CONCLUSIONS

It was shown that the combination of a bilens interferometer based of CRLs for focusing SR beams with symmetric Laue diffraction in a single crystal opens new possibilities for precise measurements of both the crystal parameters and the phase difference between the WFs in different foci of the interferometer. The phase difference can be formed by inserting microscopic objects or large objects with microscopic violations of material density.

In fact the method proposed is a new modification of the phase contrast method, in which the inverse problem is solved extremely simply. Although the number of interference bands cannot be made arbitrarily large, even several peaks at the center are sufficient to obtain useful physical information with a rather high accuracy. The proposed method can be widely used in many fields of science and technology: from physics of materials to biophysics.

FUNDING

V.G. Kohn acknowledges the support of the Russian Foundation for Basic Research, project no. 19-29-12043mk, in the part of the development of a computer program and the support of the Ministry of Science and Higher Education of the Russian Federation (grant no. 075-15-2021-1362) in the part of carrying out the computer experiment. The work of I.A. Smirnova was fulfilled within the State assignment for the Institute of Solid State Physics of the Russian Academy of Sciences.

CONFLICT OF INTEREST

The authors declare that they have no conflicts of interest.

REFERENCES

1. M. Born and E. Wolf, *Principles of Optics* (Cambridge Univ. Press., 2002).
2. A. Snigirev, I. Snigireva, V. Kohn, et al., Phys. Rev. Lett. **103**, 064801 (2009). https://doi.org/10.1103/PhysRevLett.103.064801
3. A. Snigirev, I. Snigireva, V. Kohn, et al., AIP Conf. Proc. **1365**, 285 (2011). https://doi.org/10.1063/1.3625360
4. A. Snigirev, I. Snigireva, M. Lyubomirskiy, et al., Opt. Express **22**, 25842 (2014). https://doi.org/10.1364/OE.22.025842
5. M. Lyubomirskiy, I. Snigireva, V. Kohn, et al., J. Synchrotron Radiat. **23**, 1104 (2016). https://doi.org/10.1107/S160057751601153X
6. D. Zverev, I. Snigireva, V. Kohn, et al., Opt. Express **28**, 21856 (2020). https://doi.org/10.1364/OE.389940
7. D. A. Zverev, V. G. Kohn, V. A. Yunkin, et al., Proc. SPIE **11493**, 114930L1 (2020). https://doi.org/10.1117/12.2568687
8. A. Snigirev, V. Kohn, I. Snigireva, and B. Lengeler, Nature **384**, 49 (1996). https://doi.org/10.1038/384049a0
9. V. V. Lider, Usp. Fiz. Nauk **184**, 1217 (2014). https://doi.org/10.3367/ufne.0184.201411e.1217
10. N. Kato and A. R. Lang, Acta Crystallogr. **12**, 787 (1959). https://doi.org/10.1107/S0365110X59002262
11. N. Kato, Acta Crystallogr. **14**, 526 (1961). https://doi.org/10.1107/S0365110X61001625
12. N. Kato, Acta Crystallogr. **14**, 627 (1961). https://doi.org/10.1107/S0365110X61001947
13. M. K. Balyan, Acta Crystallogr. A **66**, 660 (2010). https://doi.org/10.1107/S0108767310035944
14. V. G. Kohn and I. A. Smirnova, Kristallografiya **67** (2), 185 (2022). https://doi.org/10.31857/S0023476122020084
15. A. M. Afanas'ev and V. G. Kon, Sov. Phys. Solid State **19** (6), 1035 (1977).
16. V. G. Kohn, Kristallografiya **24**, 712 (1979).

17. A. A. Aristov, V. I. Polovinkina, I. M. Shmyt'ko, and E. V. Shulakov, Pis'ma Zh. Eksp. Teor. Fiz. **28**, 6 (1978).
18. V. D. Koz'mik and I. P. Mikhailyuk, Pis'ma Zh. Eksp. Teor. Fiz. **28**, 673 (1978).
19. V. V. Aristov, V. I. Polovinkina, A. M. Afanasev, and V. G. Kohn, Acta Crystallogr. A **36**, 1002 (1980). https://doi.org/10.1107/S0567739480002045
20. V. V. Aristov, V. G. Kon, and A. A. Snigirev, Sov. Phys. Crystallogr. **31** (6), 626 (1986).
21. V. V. Aristov, A. A. Snigirev, A. M. Afanasev, et al., Acta Crystallogr. A **42**, 426 (1986). https://doi.org/10.1107/S0108767386098926
22. M. Hurt and A. D. Milne, Acta Crystallogr. A **26**, 223 (1970). https://doi.org/10.1107/S056773947000058X
23. http://xray-optics.ucoz.ru/XR/xrwp.htm
24. V. G. Kohn, J. Synchrotron Radiat. **23**, 615 (2022). https://doi.org/10.1107/S1600577522001345
25. J. W. Cooley and J. W. Tukey, Math. Comput. **19**, 297 (1965).
26. http://kohnvict.ucoz.ru/jsp/3-difpar.htm
27. A. Authier, *Dynamical Theory of X-ray Diffraction* (Oxford Univ. Press, 2005).
28. A. C. Kak and M. Slaney, *Principles of Computerized Tomographic Imaging* (IEEE Press, 1988).
29. V. G. Kohn and T. S. Argunova, Phys. Status Solidi B **259** (4), 2100651 (2022). https://doi.org/10.1002/pssb.202100651

Translated by Yu. Sin'kov